Manipulator design for a haptic system with improved performance

Veysel Sekendiz[1], İbrahimcan Görgülü[1], Mehmet Görkem Karabulut[1], Gökhan Kiper[1], Mehmet İsmet Can Dede[1]

[1] Department of Mechanical Engineering, İzmir Institute of Technology
Email: {mehmetsekendiz, ibrahimcangorgulu, mehmetkarabulut, gokhankiper, candede}@iyte.edu.tr

Abstract

This paper presents the work carried out to improve the design of an existing kinesthetic haptic device. The proposed improvement is designated for enhancing this device's impedance width which is a common metric in performance evaluation of haptic devices. In this study, kinematic design optimization, static balancing, constructional design enhancement and actuation system design studies are presented.

Keywords: Haptic device, parallel manipulator, impedance width, transparency, manipulator stiffness

1 Introduction

A teleoperation system is composed of a master system on the human operator site, a slave system on the task site and a communication infrastructure between these two systems. Generally, the master system is distant from the task site and human operator accomplishes the task using the master system by sending commands to use the slave system. Usually, the mentioned commands are motion commands and the master system is responsible for acquiring these motion commands from the human operator. Depending on the necessities of the task, the mentioned motion commands are acquired by sensing generally the hand motion and sometimes sensing the foot, leg, eye or total body movement of the human operator.

In the teleoperation system, if the slave system's physical interaction information with the task site is to be sent to the master system as force-feedback, then the master system is required to transmit this fed-back force information to the human operator. The devices that both acquire the motion of the desired limbs of the human operator and provide the force transmission to the human operator are called kinesthetic haptic devices.

This study is part of work done for the project titled "design of a Haptic system with Improved performance via developing its new Sub-Systems (HISS)". The HISS project aims to propose a new mechanism, new sub-components and model improvements in desktop haptic device technology. The manipulator is to serve as the master device in precision required teleoperation tasks. The manipulator to be used is selected as the R-CUBE mechanism [1] which is a 3-degree-of-freedom 3-legged translational parallel manipulator with 5R limbs where the revolute joint at the base has parallel axis to the next revolute joint axis and the remaining 3 axes are parallel to each other and orthogonal to the first two. The 3 revolute joint axes or the 3 limbs on the base are mutually perpendicular to each other. While the R-CUBE mechanism has a

translational mobile platform, a wrist mechanism can be installed on the platform in order to control the orientation as well. This kinematic architecture has been previously used for a haptic device (Fig. 1) [2]. In this initial design, one of the ground-fixed joints of the parallelogram of each leg is coupled with a direct-drive actuation system and the other one is coupled with an angular position sensor. The links are manufactured from an Aluminum alloy and the joint structures are built by using double bearings. On the mobile platform, depending on the need, a handle or a passive wrist mechanism can be placed to change the degree-of-freedom of measuring the pose of the handle from 3 to 6. Also, the manipulator can be re-oriented from the orientation that appears in the CAD drawing in Fig. 1.a to the orientation in which one of the axes of operation is aligned with the gravity vector as shown in Fig. 1.b.

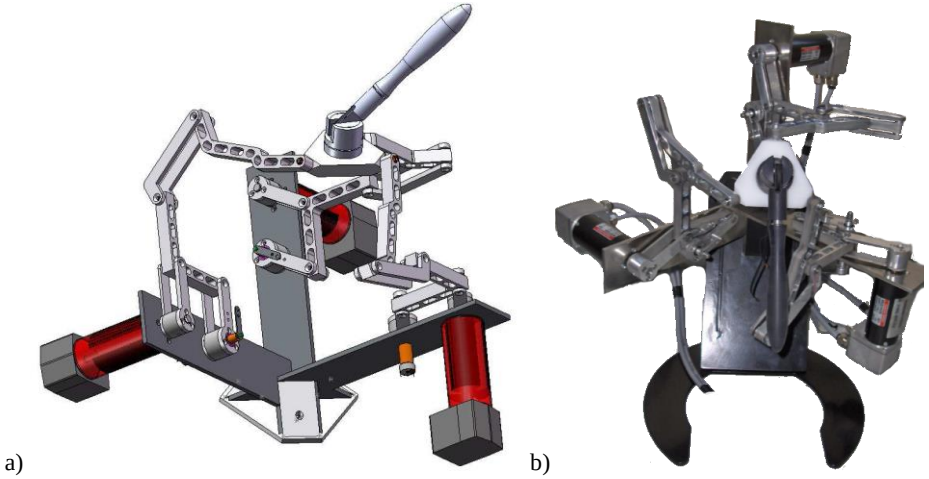

a) b)

Figure 1: HIPHAD v1.0 a) CAD model, b) real model [3]

The performance of a kinesthetic haptic device can be assessed by a number of different metrics. In [4], these metrics are categorized into three parts as unpowered, powered and control system properties. Nevertheless, the overall design of a kinesthetic device is evaluated based on its impedance width and transparency. Impedance width which was introduced in [5] is the difference between the minimum and maximum mechanical impedance that can be displayed by haptic device. The minimum impedance is a measure of resistance to free motion that is felt by the human operator when he/she tries to back-drive the haptic device. This performance is affected adversely by the friction at the joints and the moved mass/inertia. The maximum impedance is the measure of the maximum resistance that can be displayed by the device to the back-driving motion of the human operator. Based on the impedance width performance criterion, the major problems of the initial design can be listed as:

(1) links are constructed to have relatively larger mass and inertia, which results in increasing the minimum impedance.
(2) direct-drive actuation limits the maximum torque that can be generated in a limited area, which results in decreasing the maximum impedance.

(3) joint structures are constructed by using low-friction bearings, which results in decreasing the maximum impedance since the stability of the device when displaying larger impedance is jeopardized by minimizing the physical damping [5].
(4) total number of links are more than necessary because of the use of the parallelograms, which increases the minimum impedance.
(5) link lengths are not optimized for maximizing the stiffness, which affects both minimum and maximum impedance adversely.
(6) the manipulator is not passively balanced for gravitational effects, which limits the performance of the actuators that are working against gravitational effects thus, decreases the maximum impedance.

A measurement of the impedance characteristics of the initial design was presented in [6]. This study presents the work done in mechanical and actuation aspects to improve impedance width performance of the R-CUBE kinematic architecture to be used as a high performance haptic device. The design studies presented in this paper are listed as the kinematic design, static balancing, constructional design and semi-active actuator design.

2 Manipulator Architecture and Kinematic Design

Fig. 2 depicts the components and kinematic parameters of the modified version of the R-CUBE mechanism. The parallelogram loops in version 1 (Fig. 1) do not exist in version 2. Also the link lengths are modified as explained in further sections.

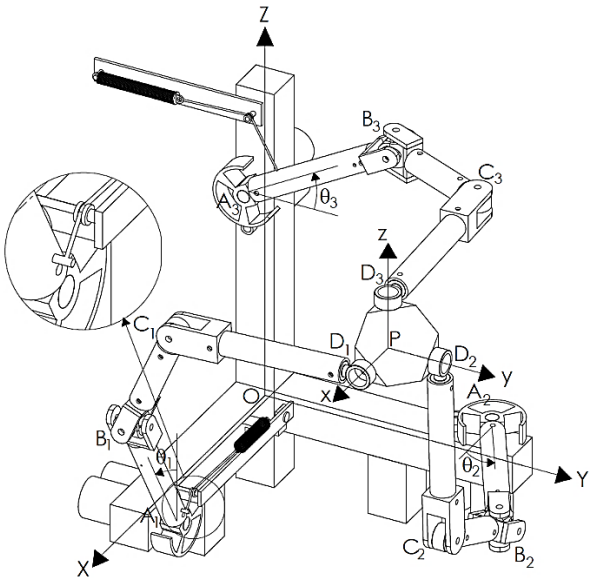

$|OA_1| = |OA_2| = |OA_3| = a$

$|A_1B_1| = |A_2B_2| = |A_3B_3| = b$

$|B_1C_1| = |B_2C_2| = |B_3C_3| = c$

$|C_1D_1| = |C_2D_2| = |C_3D_3| = d$

$|D_1P| = |D_2P| = |D_3P| = e$

Figure 2: HISS Kinematic Parameters

The manipulator comprises identical legs attached to 3 mutually orthogonal axes. Joints A_i, C_i, D_i are revolute joints, whereas joints B_i are universal joints for i = 1, 2, 3. Link

length parameters are depicted in Fig. 2. A fixed frame O(X, Y, Z) is attached to the fixed link and a moving frame P(x, y, z) is attached to the mobile platform. Since the manipulator is a translational manipulator, the P(x, y, z) frame axes remain parallel to the O(X, Y, Z) frame axes at all times. Due to the kinematic architecture of the manipulator, $B_1C_1D_1$, $B_2C_2D_2$ and $B_3C_3D_3$ define planes attached to the mobile platform perpendicular to x-, y- and z-axes, respectively. The locations of these planes with respect to the O(X, Y, Z) frame are determined by the A_iB_i links. Therefore, Leg 1 ($A_1B_1C_1D_1$) is responsible for the motion of the platform along the x-axis and similarly Leg 2 and Leg 3 are responsible for the motion of the platform along the y- and z-axes, respectively. As a result of this architecture, the workspace of the end-effector point P is cubic.

The forward/inverse kinematics formulation of the R-cube manipulator is very simple and very few link lengths need to be determined for the rigid-body kinematics, while several other link lengths are arbitrary for kinematic relations assuming rigid links and joints. It is desired that the end-effector point P is at the center of the cubic workspace when A_1B_1, A_2B_2 and A_3B_3 are perpendicular to the X-, Y- and Z-axes, respectively. This is the home position of the manipulator. Actuated joint angles θ_i are measured from the A_iB_i locations at the home position as depicted in Fig. 2. In order for point P to be at the center of the cubic workspace at the home position, $|A_iB_i| = b = a - e$. The forward kinematics equations are easily obtained as follows:

$$P_x = b(1 + \sin\theta_1) \tag{1}$$
$$P_y = b(1 + \sin\theta_2) \tag{2}$$
$$P_z = b(1 + \sin\theta_3) \tag{3}$$

Consequently, the inverse kinematics equations are obtained as

$$\theta_1 = \sin^{-1}\left(\frac{P_x}{b} - 1\right) \tag{4}$$
$$\theta_2 = \sin^{-1}\left(\frac{P_y}{b} - 1\right) \tag{5}$$
$$\theta_3 = \sin^{-1}\left(\frac{P_z}{b} - 1\right) \tag{6}$$

Accordingly, the forward kinematics Jacobian matrix $\hat{J}$ is obtained as

$$\hat{J} = \begin{bmatrix} b\cos\theta_1 & 0 & 0 \\ 0 & b\cos\theta_2 & 0 \\ 0 & 0 & b\cos\theta_3 \end{bmatrix} \tag{7}$$

Since HISS is designed to be used as a haptic device, the dimensional synthesis of the modified R-CUBE mechanism is conducted in accordance with the haptic performance metrics. The performance of a haptic manipulator is determined by its mechanical impedance characteristics since it designates the quality of the reflected force/torque to the user. The range between the maximum and minimum value determines the range of forces/torques to be rendered while the frequency range indicates the diversity of the forces/torques which is felt by the user. Hence, higher range in both the impedance and frequency is needed to enhance the perception of

reality and quality of the performance. However, impedance and the frequency range depend on the performance of kinematics, stiffness and dynamics characteristics which are highly contradicted with each other. Higher stiffness is required to render higher impedances. However, increasing the stiffness performance is achieved by driving the manipulator to singular poses and/or increasing the thickness of the links. In both cases, either kinematic performance is decreased in terms of manipulability or dynamic performance is decreased which reduces the performance of minimum impedance. Therefore, an optimization is required to determine the kinematic parameters by virtue of kinematics, stiffness, and dynamic performance metrics. Since the relationship between these metrics is non-linear, evolutionary or artificial intelligence based optimization algorithms are needed. In this study, the multi-objective genetic algorithm is adopted for optimization. In order to construct the objective functions, kinematic, stiffness, and dynamic models are procured. In kinematic performance evaluation, manipulability [7] and condition number [8] are the optimization parameters for achieving singularity avoidance and isotropic motion resolution distribution within the workspace. Next, the stiffness model is obtained by using the virtual joint method [9] and represented by means of a stiffness matrix in the Cartesian space, $\widehat{K}_C$. The computation is achieved by the multiplication of $\widehat{K}_C = (\hat{J}_\theta \widehat{K}_\theta^{-1} \hat{J}_\theta^T)^{-1}$, where $\hat{J}_\theta$ is the Jacobian matrix including the virtual joint variables and $\widehat{K}_\theta$ denotes the stiffness matrix in joint space which is only depend on the geometry and mechanical properties of the links. The determinant of the stiffness matrix, which is pose dependent, is computed in order to obtain the measure of rigidity as a scalar metric [10]. Finally, determinant of the inertia matrix of the modified R-CUBE is calculated in order to obtain the mass distribution with respect to pose changes. The aim is to increase the manipulability and stiffness while decreasing the inertia and condition number. The objective functions to be minimized are constructed as follows

$$O_1 = \left|\hat{J}\right|^{-1} \tag{8}$$

$$O_2 = \left\|\hat{J}\right\| \left\|\hat{J}^{-1}\right\| \tag{9}$$

$$O_3 = \left|\widehat{M}_C\right| \tag{10}$$

$$O_4 = \left|\widehat{K}_C\right|^{-1} \tag{11}$$

where | | is the determinant and || || is the 2-norm operator and $\widehat{M}_C$ and $\widehat{K}_C$ are the pose dependent inertia and stiffness matrices in Cartesian space. O_1, O_2, O_3, and O_4 are the inverse of manipulability index, condition number, the determinant of the inertia matrix and the inverse of the determinant of the stiffness matrix, respectively. The links are assumed to be made of carbon fiber composite tubes with 10 mm outer and 6 mm inner diameter, hence associated mass and stiffness values are used. Constraint equations are introduced to the optimization algorithm in order to avoid singularity. An extra constraint is added for ergonomics so that the hand of the user does not collide with any of the links. The optimization is conducted by Pareto-front approach. Hence, a set of optimum solutions is obtained and the one which has the highest impedance and natural frequency is selected. Optimum solution parameters are as b = 111.7 mm, c = 74.1 mm, d = 121.8 mm. In this case, the maximum range of the input joints are ±32.5° and the values of objective functions are computed to as , $O_1 = 10.638$, $O_2 = 10.63, O_3 = 51 \times 10^{-4}$, and $O_4 = 8.821 \times 10^{-7}$.

3 Constructional Design and Balancing

It is important to have a light-weight and high stiffness manipulator to have high transparency and high frequency range in impedance type of haptic device. Therefore, carbon fiber composite tubes and aluminum connections are selected as the materials for the links (Fig 3).

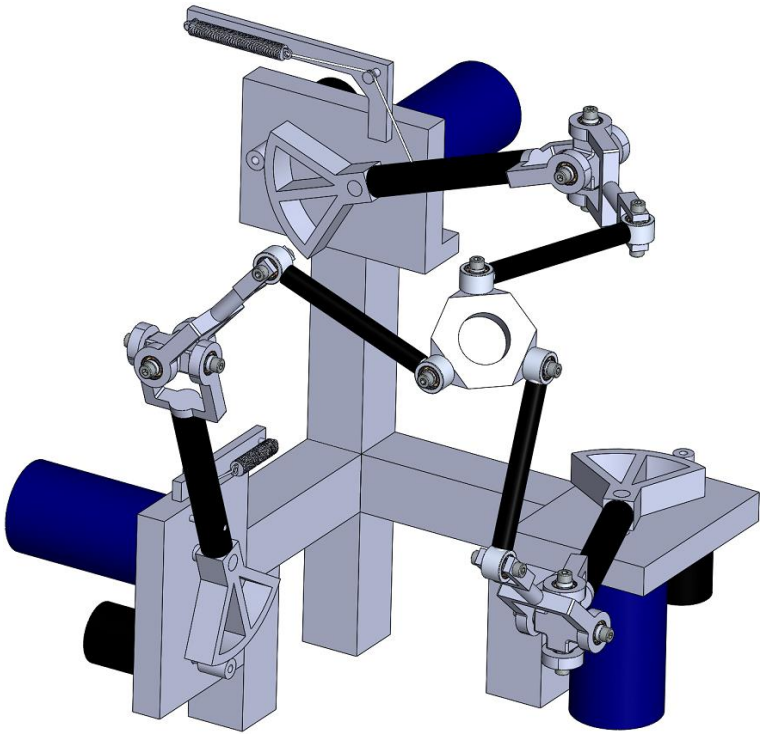

Figure 3: HISS CAD Design

When using a manipulator as a master device, the operator should not feel the weight and inertial effects of the links. For gravity compensation, springs are designed. The weights of the moving platform and all links that move in the same z-level with the moving platform are lumped to Leg 3, which is responsible for the z-axis motion and balanced with a single spring attached to the driving link A_3B_3 of Leg 3. The potential energy of the platform and links B_3C_3 and C_3D_3 change together, so their masses are added up and lumped to joint B_3. Also, to simplify the balancing solution, half of the masses of links B_1C_1, C_1D_1, B_2C_2 and C_2D_2 are added to the aforementioned lumped mass as well. The reason for taking the half of mass for theses links is that the mass centers of these links are approximately at the middle and hence the z-motion of these centers of masses are approximately half of that of the platform. Let M denote the whole lumped mass. Then

$$M = m_P + m_c + m_d + 2(m_c/2) + 2(m_d/2) = m_P + 2m_c + 2m_d \qquad (12)$$

where m_c, m_d and m_P are masses of the platform, link B_iC_i and link C_iD_i, respectively. Also considering the mass m_b of the driving link A_3B_3, the inverted pendulum shown in Fig. 4 needs to be balanced.

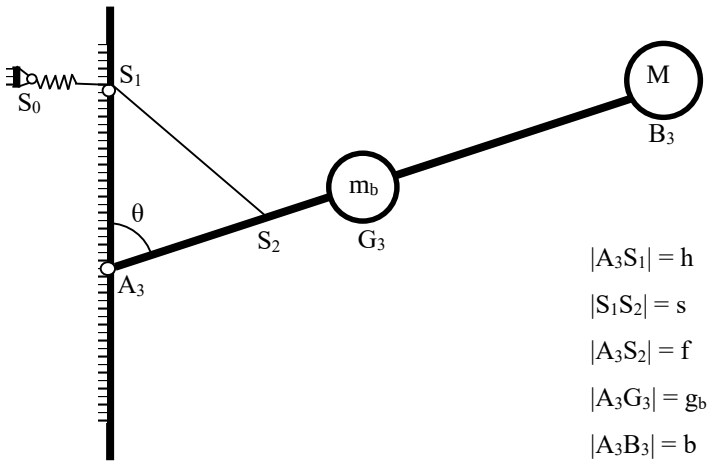

Figure 4: Spring balancing

The spring attachment point location or the length of the string attached to the spring should be adjusted such that the spring is unloaded when θ = 0, i.e. when link A_3B_3 is at upright position. $|A_3S_2|$ = f, $|A_3S_1|$ = h and spring constant k are design parameters. The total potential energy of the masses and the spring can be written as

$$U = m_b g g_b \cos\theta + Mgb\cos\theta + \frac{1}{2}ks^2 \qquad (13)$$

Cosine theorem in triangle $S_1S_2A_3$ reads

$$s^2 = f^2 + h^2 - 2fh\cos\theta \qquad (14)$$

In order to have constant potential energy, its variation with respect to θ should be zero. Substituting Eq. (14) in Eq. (13), differentiating and equating to zero:

$$\frac{\partial U}{\partial \theta} = (-m_b g g_b - Mgb + kfh)\sin\theta = 0 \Rightarrow kfh = (m_b g_b + Mb)g \qquad (15)$$

All terms on the right-hand side of Eq. (15) are known. First for chosen f and h, a desired k value is determined. Then a tension spring is manufactured according to the desired k value. The spring constant of the manufactured spring is then determined with several tests. The measured spring constant is usually different from the desired value. f or h value is adjusted according to the measured k value.

The only remaining unbalanced link is link A_1B_1. This link can also be balanced individually with a similar approach. The balance springs for the new design are illustrated in Figs. 2 and 3. To test the balancing performance, High Precision Haptic Device (HIPHAD) version 1 shown in Fig. 1 is balanced with two springs (Fig. 5). The tests show that the moving platform remains in static balance wherever the operator positions it when the actuators are not active.

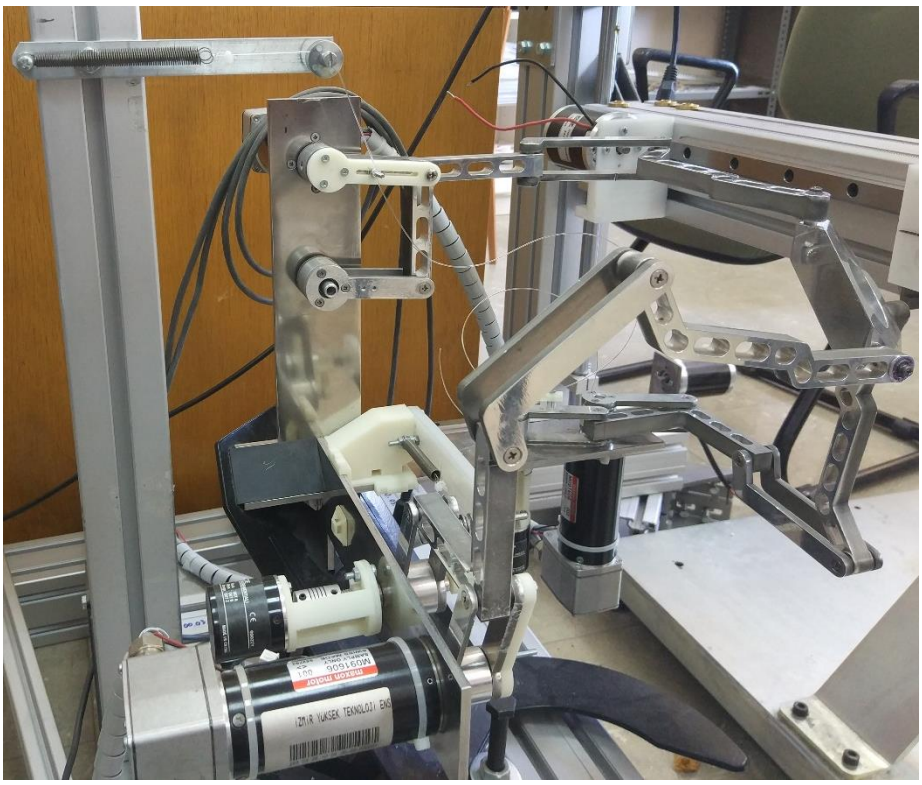

Figure 5: Spring balanced HIPHAD v1.0

4 Semi-Active Actuator Design

A haptic device does not only work to display constraints to stimulate the human operator but it also produces motion of the handle to stimulate effects such as surface roughness or slip conditions. In the previous version of the device the actuation system was composed of a direct-drive system that included a BLDC motor. An actuation system composed in this way or by combining an electrical motor with a reduction system such as Capstan drive enables to display both constraints and motion at the handle of the device. However, although these actuation systems are designed for producing motion, applying brakes with these actuation systems to display constraints have a limiting factor. This limiting factor is the size of the actuator. In order to display

larger amount of static forces, larger electric motors are required which degrade the dynamic performance of the system.

In haptic device development, MR-fluid based brake systems can produce controllable viscosity-based damping force. A design of an MR-brake based haptic device is introduced in [11] and a multi degree-of-freedom haptic device was built by using an MR-fluid brake [12]. Some researchers even used the MR-brakes with the conventional motor-capstan drive systems [13] to increase the z-width of the device by increasing the maximum stiffness of the system.

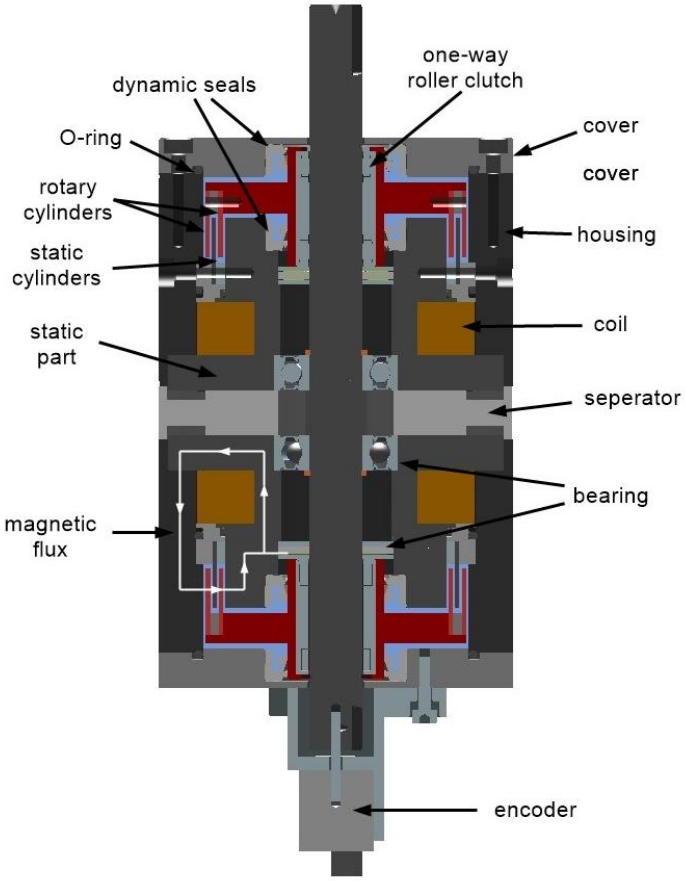

Figure 6: Design details of the bi-directional MR-brake system [16]

A magneto-rheological (MR) fluid based semi-active actuation system or in other words, an MR-fluid based brake system is designed to resolve this problem of displaying larger amount of static forces without jeopardizing the dynamic performance of the system. There are two major disadvantages of such systems;

(1) it cannot be the sole actuation system in a haptic device is the device is required to display motion like in the solution given in [14].

(2) the conventional design of a rotary MR-fluid based brake applies brake in both directions when it is activated. This results in an undesired stiction feeling displayed to the human user.

The design proposed has two rotary MR-brakes assembled on top of each other to constrain the motion of a common shaft in between them in opposite directions. In this way, decoupled way of braking is possible and thus, the stiction problem is resolved [15]. The design and its performance evaluation is provided in [16] and presented in Fig. 6.

The key element in the design is the one-way clutch or in other words, one-way bearing, which constrains the motion in one direction lets it free in the other. This new MR brake design has two directional brake conditions as presented in Fig. 7:

(1) The rotation in the clockwise direction:
- Top rotating part of the MR-brake and the shaft are coupled
- The human operator feels the braking torque with the activation of top part of the MR brake
- Free rotation is in reverse direction, even the brake is activated for the top part

(2) The rotation in the counterclockwise direction:
- Bottom rotating part of the MR-brake and the shaft are coupled
- The human operator feels the braking torque with the activation of bottom part of the MR brake
- Free rotation is in reverse direction, even the brake is activated for the bottom part

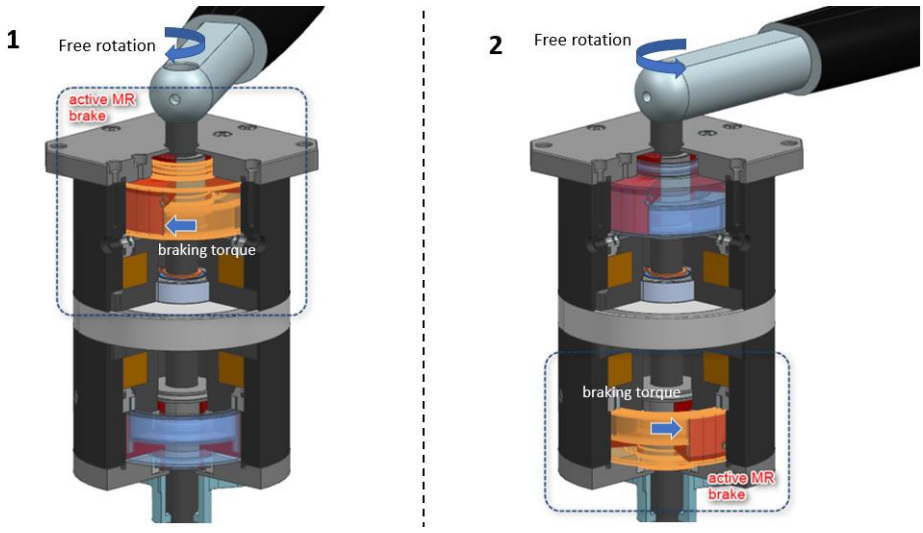

Figure 7: Bi-directional operation of the new MR-brake system

As a result of this design, brake can be applied in only one direction and even motion in both directions can be constrained simultaneously at different braking torques. The

results from an experimental study presented in Fig. 8 clearly indicates that when the MR-brake constrains the motion in one direction, the user is free to move in the other direction.

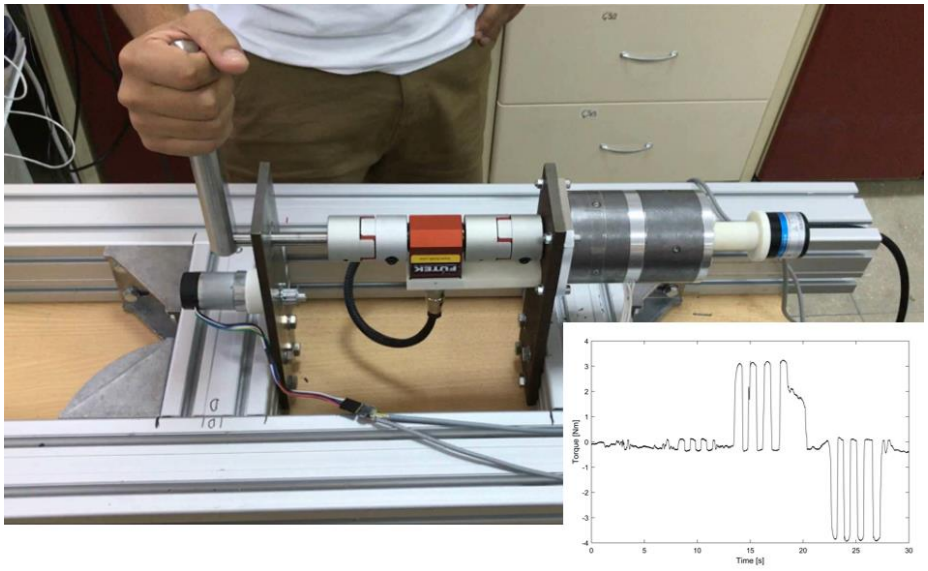

Figure 8: User evaluation test set-up and the result

Table 1. Bi-directional MR-brake specifications [16]

Category	**Specification**
Product mass	3.57 kg
Braking torque @ 2 A	3.8 N·m
Off-state torque	0.15 – 0.4 N·m
Bandwidth	63 rad/s
External Diameter	80 mm
Length	124 mm
Coil wire dia.	0.5 mm
Max. operational current	2 A
Number of turns (coil)	450
Magneto-rheological material	MRF-122EG
Magnetic material	AISI 1008 Steel
Non-magnetic material	Stainless Steel and Aluminium

The experimental test setup in Fig. 8 is composed of a handle attached to the MR-brake via a torque sensor. The user moves the handle in both directions during the test. The plot on the bottom right corner is for the measured torques by the torque sensor as the user moves the handle. After a while, the MR-brake is activated in one direction then, it is activated in the other direction and finally, they are both in off condition to terminate the experiment. It is clearly observed from this plot that the user's motion is

constrained by a maximum torque when he tries to move in the direction of the constraint and when he moves in the other direction, the measured torque is minimized. This result proves the working principle of the bi-directional MR-brake system. A study is carried out to characterize the developed system. The results of this characterization is presented in Table 1.

5 Conclusions

This study presents the mechanical design of a manipulator to be used for a haptic system that can acquire accurate motion demand even when it is providing force feedback and that has enhanced impedance width and transparency performance. First, the kinematic parameters are optimally designed according to kinematic, stiffness and dynamic performance indices. Then a lightweight and statically balanced constructional design is presented. Finally, the semi-active actuator design is given. Manufacturing and tests of the prototype of the designed manipulator are the future works for this study.

Acknowledgments
This work is supported by The Scientific and Technological Research Council of Turkey via grant number 117M405.

References

1. W. Li, F. Gao, J. Zhang, “R-CUBE, a decoupled parallel manipulator only with revolute joints”, Mechanism and Machine Theory, 40, 2005, 467–473.
2. T. Bilgincan, E. Gezgin, M. İ. C. Dede, “Integration of the hybrid-structure haptic interface HIPHAD v1.0’’, Proc. Int. Sym. Mechanism and Machine Theory, Izmir, Turkey, 267-284, 2010.
3. T. Bilgincan, “Design of a Six Degree-of-Freedom Haptic Hybrid Platform Manipulator’’, MSc Thesis, İzmir Institute of Technology, İzmir, Turkey, May 2010.
4. E. Samur, Performance Metrics for Haptic Interfaces, Springer, 2012.
5. J. E. Colgate, J. B. Brown, “Factors affecting the z-width of a haptic display”, Proc. IEEE Int. Conf. Robotics and Automation, 3205–3210, 1994.
6. E. Mobedi, İ. Görgülü, M. İ. C. Dede, “Experimental evaluation of actuation and sensing capabilities of a haptic device”, accepted to be presented in European Conf. Mechanism Science (EUCOMES), Aachen, Germany, 2018.
7. T. Yoshikawa, “Manipulability of robotic mechanisms”, International Journal of Robotics Research, 4(2), 1985, 3-9.
8. J. K. Salisbury, J. J. Craig, “Articulated hands: force control and kinematic issues”, International Journal of Robotics research, 1(1), 1982, 4-17.
9. C. Gosselin, "Stiffness mapping for parallel manipulators," IEEE Transactions on Robotics and Automation, vol. 6, no. 3, pp. 377-382, 1990.
10. G. Carbone, M. Ceccarelli, “Comparison of indices for stiffness performance evaluation”, Frontiers of Mechanical Engineering, 5(3), 2010, 270-278.
11. B. Liu, W. Li, P. B. Kosasih, and X. Zhang, "Development of an MR-brake-based haptic device," Smart materials and structures, vol. 15, no. 6, p. 1960, 2006.

12. D. Senkal and H. Gurocak, "Spherical brake with MR fluid as multi degree of freedom actuator for haptics," Journal of Intelligent Material Systems and Structures, vol. 20, no. 18, pp. 2149-2160, 2009.
13. E. Samur, L. Flaction, U. Spaelter, H. Bleuler, D. Hellier, and S. Ourselin, "A haptic interface with motor/brake system for colonoscopy simulation," in Haptic interfaces for virtual environment and teleoperator systems, 2008. haptics 2008. symposium on, 2008, pp. 477-478: IEEE.
14. C. Rossa, J. Lozada, and A. Micaelli, "Design and control of a dual unidirectional brake hybrid actuation system for haptic devices," IEEE transactions on haptics, vol. 7, no. 4, pp. 442-453, 2014.
15. M. Karabulut, B. Taner, and M. Dede, "MR Sıvısı ile Çalışan Haptik Kol Tasarımı-Design of MR-fluid based Haptic Paddle," TOK 2015 Bildiri Kitabı, pp. 867-872, 2015.
16. M. G. Karabulut, M. I. C. Dede, “Design and experimental validation of an MR-fluid based brake for use in haptics”, Proc. Actuators 2018, Bremen, Germany, 2018.